Journal of Power Sources 273 (2015) 530–537

Contents lists available at ScienceDirect

Journal of Power Sources

journal homepage: www.elsevier.com/locate/jpowsour

Performance of vertically oriented graphene supported platinum–ruthenium bimetallic catalyst for methanol oxidation

Zheng Bo*, Dan Hu, Jing Kong, Jianhua Yan, Kefa Cen

State Key Laboratory of Clean Energy Utilization, Department of Energy Engineering, Zhejiang University, Hangzhou, Zhejiang Province 310027, China

HIGHLIGHTS

- Performance of VG supported Pt–Ru catalyst toward MOR was first reported.
- Dependence of Pt molar ratio in Pt–Ru/VG on electrolyte composition was explored.
- Pt–Ru/VG presented higher catalyst loading and smaller catalyst size than Pt–Ru/CP.
- An optimum Pt molar ratio was clarified for enhanced activity and stability.
- Pt–Ru/VG showed improved electrocatalytic properties toward MOR.

ARTICLE INFO

Article history:
Received 21 July 2014
Received in revised form
15 September 2014
Accepted 19 September 2014
Available online 28 September 2014

Keywords:
Direct methanol fuel cells
Methanol oxidation
Electrocatalysis
Vertically oriented graphene
Bimetallic catalyst

ABSTRACT

This work reports the electrocatalytic performance of vertically oriented graphene (VG) supported Pt–Ru bimetallic catalysts toward methanol oxidation reaction (MOR). Dense networks of VG are directly synthesized on carbon paper (CP) *via* a microwave plamsa-enhanced chemical vapor deposition (PECVD) method. A repeated pulse potentials approach is applied in a conventional three-electrode electrochemical system for the co-electrodeposition of Pt–Ru bimetallic nanoparticles. It is found that, the decoration of VG can simultaneously lead to a ~3.5 times higher catalyst mass loading and a ~50% smaller nanoparticle size than the pristine CP counterparts. An optimum Pt molar ratio of 83.4% in the deposits, achieved with a $[H_2PtCl_6]$:$[RuCl_3]$ of 1:1 in the electrolyte, is clarified with synthetically considering the mass specific activity, CO tolerance, and catalytic stability. According to Tafel analysis and cyclic voltammetry (CV) tests, the Pt–Ru/VG catalyst with the optimized Pt molar ratio can realize a faster methanol dehydrogenation than Pt/VG, and present a significantly enhanced catalytic activity (maximum current density of 339.2 mA mg^{-1}) than those using pristine CP and Vulcan XC-72 as the supports.

1. Introduction

Direct methanol fuel cells (DMFCs) are commercially attractive due to the significant advantages beyond external reformation-hydrogen counterparts in the handling, transportation, and storage of fuels. In DMFCs, methanol is directly fed into the unit without any complex prior-reforming process, and thus can largely simplify the fuel cell system [1,2].

Considering the slow kinetics of methanol oxidation reaction (MOR), the exploration and development of effective anode catalysis deserve continuous scientific endeavors to be directed toward [3]. The pioneering work on platinum (Pt) based catalysis of MOR can be dated back to the 1960s [4], followed by the investigation on binary and ternary metallic catalysts (Pt based alloys) since the mid-1970s [5]. Now platinum–ruthenium (Pt–Ru) bimetallic catalyst has been widely recognized as one of the most preeminent candidates for operating MOR with a high efficiency [2,5,6]. Research on the kinetics of MOR over Pt and Pt–Ru catalysts reveals that an adequate addition of Ru could lead to an enhanced catalyst activity, mainly attributed to both the bi-functional mechanism and the ligand effect [3,7,8]. Typically, active OH_{ads} species can be produced at a relatively low potential with the presence of Ru, benefiting the reactions with the adsorbed intermediates on neighboring Pt sites [9,10].

On the other hand, employing high-performance catalyst support is considered as a promising strategy for enhanced dispersion and utilization of nanosized catalysts. As reviewed by Zhao et al. [9],

* Corresponding author at: State Key Laboratory of Clean Energy Utilization, Institute for Thermal Power Engineering, Department of Energy Engineering, Zhejiang University, 38 Zheda Road, Zhejiang 310027, China. Tel.: +86 571 87953290; fax: +86 571 87952438.
E-mail addresses: bozh@zju.edu.cn, zjuzhengbo@gmail.com (Z. Bo).

http://dx.doi.org/10.1016/j.jpowsour.2014.09.125
0378-7753/

Cuenya [11], Liu et al. [12], and Sharma et al. [13], various nanostructured carbonaceous or inorganic oxide/carbide supports have been proposed aiming at an improved catalyst performance in MOR. Among which, oriented carbonaceous nanostructures built from sp^2 hybridized carbon atoms have emerged as promising alternatives. Typically, vertically aligned carbon nanotubes (VCNTs) and vertically aligned carbon nanofibers (VCNFs) were demonstrated as promising supports for a better dispersion of Pt nanoparticles than that of Pt/graphite, thus exhibiting higher electrocatalytic activity [14,15]. The development of plasma-enhanced chemical vapor deposition (PECVD) technique allows the expansion of above advantages from one-dimensional (1D) CNTs and CNFs to two-dimensional (2D) graphene. Our recent review summarized the growth of vertically oriented graphene (VG) with various plasma sources and different operating parameters [16]. Compared with Pt/VCNF and conventional Pt/C electrodes, Pt/VG presented a superior electrocatalytic activity due to VG's unique orientation, exposed sharp edges, non-stacking morphology, and huge surface-to-volume ratio [17,18]. Different with the graphene nanosheets produced by traditional chemical methods which are easily restacked due to the strong van der Waals interactions, networks of VG directly synthesized on the substrate *via* PECVD method present a non-stacking morphology and exposed graphene surface, benefiting the utilization of graphene's high specific surface area for catalyst loading. Meanwhile, the exposed edge planes of VG will help the nucleation, dispersion, and immobilization of Pt nanoparticles [19,20]. Finally, the unified vertical orientation of VG favors the electron transport due to the significantly (~10^5 times) higher in-plane than out-of-plane electrical conductivity of graphene [17,21]. However, to the best of our knowledge, the performance of VG supported Pt–Ru catalyst for MOR has yet been reported in detail.

In this paper, co-electrodeposition of Pt–Ru bimetallic catalyst on VG-coated carbon paper (CP) was conducted with a repeated pulse potentials approach. The catalyst loading mass, nanoparticle size, and nanoparticle dispersion on VG-coated CP were characterized and compared with those on pristine CP. With using VG-coated CP as the support, the influence of electrolyte composition (*i.e.*, H_2PtCl_6 and $RuCl_3$ concentrations) on Pt and Ru molar ratios of the deposits was clarified. The corresponding catalytic activities, CO tolerance, and stabilities of the VG supported Pt–Ru catalysts with various Pt molar ratio were investigated in detail to explore an optimum electrolyte composition. Tafel analysis was carried out to compare the MOR kinetics of VG supported Pt and Pt–Ru catalysts, and finally, the electrocatalytic performance of VG supported Pt–Ru was compared with those using CP and Vulcan XC-72 as the supports.

2. Experimental

2.1. Synthesis of VG on CP

VG networks were grown directly on a CP (9 mm × 8 mm, Toray Inc) *via* a home-made microwave-PECVD device. Microwave was confined by a waveguide with a transverse electric (TE) mode, *i.e.*, all the electric fields were transverse to the direction of propagation while no longitudinal electric field was present. CP was placed on a rounded stainless steel holder. Prior to the growth process, CP substrate was pretreated by 50 standard cubic centimeters per minute (sccm) H_2 gas for 5 min under a 350 W microwave. 10 sccm CH_4 was added into the system as a carbon source, and a 50 V bias was applied to the CP substrate for VG growth. After 2 min growth, the sample was cooled down to room temperature under the protection of H_2.

2.2. Co-electrodeposition of Pt–Ru

The electrolyte used for the co-electrodeposition of Pt–Ru nanoparticles was prepared by mixing solutions consisting of $H_2PtCl_6 \cdot 6H_2O$ (Sinopharm Chemical Reagent CO., Ltd), $RuCl_3 \cdot xH_2O$ (Sinopharm Chemical Reagent CO., Ltd), and H_2SO_4 (98%, Sinopharm Chemical Reagent CO., Ltd) in a 50 mL deionized water at room temperature. The concentration of H_2SO_4 in the electrolyte was fixed as 0.5 M. The concentration of H_2PtCl_6 ($[H_2PtCl_6]$) varied from 1 to 9 mM and the corresponding concentration of $RuCl_3$ ($[RuCl_3]$) was accordingly adjusted from 9 to 1 mM. The co-electrodeposition process was conducted at a N_2 gas saturated condition, where N_2 was employed to purge the dissolved oxygen and separate air from the electrolyte during the electrodeposition process. A repeated pulse potentials approach was performed in a conventional three-electrode electrochemical system for the co-electrodeposition of Pt–Ru. 0.7 cm^2 of catalyst support was exposed to the solution as a working electrode. A Pt foil and a saturated calomel electrode (SCE) were used as the counter electrode and reference electrode, respectively. The two repeated potentials, including a potential of −0.40 V vs. SCE for 100 ms and a potential of +0.60 V vs. SCE for 300 ms, were applied to the working electrode. The negative potential was applied for the co-electrodeposition, and the positive potential was used for metal cation diffusion in the electrolyte solutions. 300 Consecutive cycles were applied to the substrates located in working electrodes. After deposition, the specimens were thoroughly rinsed with deionized water to remove electrolyte residuals.

As for the electrodeposition of Pt–Ru nanoparticles on Vulcan XC-72 (Cabot), a pretreated bare glassy carbon (GC) disc with an exposed geometric area of 0.07 cm^2 was used as both the catalyst support and the working electrode. Prior to the electrodeposition, the carbon slurry achieved by mixing 0.5 g Vulcan XC-72 carbon powder and 1 mL Nafion solution (Sigma–Aldrich, 5 wt.% 1100 EW) with 10 mL deionized water, was put into an ultrasonic bath for 30 min after stirring thoroughly [22]. 6 μL Carbon slurry was spread on the surface of GC, followed by drying in environmental conditions for 24 h before use. The following electrodeposition procedure was the same as those for pristine CP and VG-coated CP. With using pristine CP, VG-coated CP, and commercial carbon black Vulcan XC-72 as the supports, the as-prepared catalysts were denoted as Ru–Pt/CP, Ru–Pt/VG, and Ru–CP/Vulcan, respectively.

2.3. Material characterization

The surface morphology of VG as well as the size and dispersion of Pt–Ru nanoparticles were determined by an SU-70 scanning electronic microscopy (SEM, Hitachi) and a Tecnai G2 F30 STwin transmission electron microscopy (TEM, Philips-FEI). To perform high-resolution TEM (HRTEM) characterizations, samples were wetted with ethanol and contact-transferred to a 230 mesh holey carbon grid. The crystalline structures of Pt–Ru nanoparticles were investigated by X-Ray diffraction (XRD) patterns using an XRD-6000 Diffractometer with Cu Kα source (λ = 0.15425 nm, Shimadzu). The chemical states of Pt and Ru in the catalysts were measured by an X-ray photoelectron spectroscopy (XPS, VG Escalab Mark II) with a monochromatic Mg Ka X-ray source (1253.6 eV, West Sussex). The catalyst loading mass on the support was obtained from Inductively Coupled Plasma Mass Spectrometry (ICP-MS, XSENIES, Thermo Electron Corporation) tests. The deposited specimens submitted for ICP analysis were dissolved in aqua regia at room temperature.

2.4. Electrochemical measurement

The electrochemical measurements of various catalysts were performed using an electrochemical workstation (Autolab-PGSTAT30) in a conventional three-electrode system at ambient temperature and N_2 atmosphere. To investigate the catalytic

activities of various catalysts toward MOR, cyclic voltammetry (CV) tests were carried out in a 50 mL electrolyte of 0.5 M H_2SO_4 with or without 1 M CH_3OH (scan rate: 50 mV s^{-1}, potential range: −0.2 to 1.2 V vs. SCE for H_2SO_4 and 0–1.0 V vs. SCE for H_2SO_4 + CH_3OH). For each case, the CV curve was recorded at the fifth scanning cycle. The catalyst activity was evaluated by plotting the unit mass activity, where the current densities were referred to the Pt depositions [23–25]. Chronoamperometry (CA) tests were performed to evaluate the stabilities of various catalysts, where 0.5 M H_2SO_4 + 1 M CH_3OH mixture (50 mL) was used as the electrolyte and a potential of +0.6 V vs. SCE was kept for 900 s. Tafel curves were plotted at room temperature by a linear polarization program in the electrolyte of 0.5 M H_2SO_4 + 1 M CH_3OH at a scan rate of 50 mV s^{-1}. Before each measurement, the electrolyte was purged by bubbling with purified N_2 for 30 min.

3. Results and discussion

3.1. Catalyst loading on pristine CP and VG-coated CP

Fig. 1a shows the loading mass of Pt and Ru on pristine CP with various electrolyte compositions. According to the ICP-MS tests, the Pt loading on pristine CP increased with an increasing [H_2PtCl_6] (from 1 to 9 mM), while the Ru loading reached a maximum at a [H_2PtCl_6]:[$RuCl_3$] of 1:1. The above results indicate that the reduction of Pt plays a more important role on the co-electrodeposition of Pt–Ru [26]. The total loading mass of Pt–Ru increased with the increase of [H_2PtCl_6], and the maximum value (0.096 μmol) was obtained at a [H_2PtCl_6]:[$RuCl_3$] of 9:1. Similar observation, as shown in Fig. 1b, was also obtained using VG-coated CP as the support. For the same electrolyte composition, both the loading masses of Pt and Ru on VG-coated CP were significantly higher than those on pristine CP. Typically, the maximum Pt–Ru loading on VG-coated CP could reach 0.324 μmol, almost 3.5 times higher than that on pristine CP.

Fig. 2a–f presents the SEM images of Pt–Ru/CP and Pt–Ru/VG obtained from three typical electrolyte compositions, *i.e.*, [H_2PtCl_6]:[$RuCl_3$] = 3:7, [H_2PtCl_6]:[$RuCl_3$] = 1:1, and [H_2PtCl_6]:[$RuCl_3$] = 7:3, respectively. VG nanosheets were uniformly synthesized on CP, providing dense open graphitic edge planes as additional sites (not only the edges but also the side faces) for the nucleation and growth of nanosized catalysts. As a consequence, higher catalyst loading was obtained using VG-coated CP as the support. Meanwhile, the presence of VG could prevent the surface migration and aggregation of nanoparticles [18], resulting to much smaller average size of Pt–Ru catalysts on VG-coated CP than the pristine CP counterpart (for the same electrolyte composition). As estimated from the SEM images shown in Fig. 2, the average sizes of Pt–Ru/VG were around 50% smaller than those of Pt–Ru/CP. Typical HRTEM image of Pt–Ru/VG, which was obtained with a electrolyte composition of [H_2PtCl_6]:[$RuCl_3$] = 1:1, was also provided in Fig. 2g.

3.2. Catalyst activity of Pt–Ru/VG toward MOR

Fig. 3a shows the molar ratios of Pt and Ru deposited on VG-coated CP with various electrolyte compositions. Upon increasing [H_2PtCl_6] from 1 to 9 mM, the Pt molar ratio increased from 37% to 96% and the Ru molar ratio decreased from 63% to 4% accordingly. It thus provided a facile alternative for the controllable deposition of Pt–Ru catalysts with different Pt and Ru ratios. The Pt molar ratio was found to be higher than that in the original electrolyte, in accordance with the previously reported founding [26]. Fig. 3b shows the corresponding XRD patterns of various Pt–Ru/VG catalysts obtained from different electrolyte compositions. The XRD patterns shown the diffraction peaks of Pt (111), Pt (200), Pt (220), and Pt (311), matching to the face centered cubic (fcc) structure [27]. With the decrease of [H_2PtCl_6], a slight shift of the diffraction peaks of Pt (111) to higher 2-theta and a decrease of peak intensity were observed in the patterns, probably due to the increasing Ru ratio in the deposits [28]. The peaks corresponding to the typical hexagonal closed packed (hcp) structure of Ru metal or ruthenium oxides/hydroxides were not observed, suggesting the possibility that Ru existed as alloys with Pt atoms or amorphous ruthenium hydroxides [26,28]. The Ru atomic fraction in the Pt–Ru alloy was calculated according to Vegard's law [29]. Results show that the Ru atomic fraction for all the samples ranged from 4.0% to 13.6% (typically, 12.1% for [H_2PtCl_6] = 5 mM).

XPS measurement was conducted to characterize the oxidation states of Pt and Ru. Typical Pt 4f and Ru 3p XPS spectra of the representative sample, *i.e.*, Pt–Ru/VG with the electrolyte of [H_2PtCl_6]:[$RuCl_3$] = 1:1, are shown in Fig. 3c and d. In Fig. 3c, the peaks at 74.8 and 71.6 eV are assigned to Pt $4f_{7/2}$ and Pt $4f_{5/2}$, respectively. To determine the different oxidation states of Pt, the overall doublet was deconvoluted into three pairs of peaks. The binding energy values of 71.5 and 74.7 eV, 72.2 and 75.3 eV, as well as 74.2 and 77.5 eV correspond to three different oxidation states of Pt, *i.e.*, metallic Pt(0), Pt(II) mainly in PtO or $Pt(OH)_2$ species, and Pt(IV) generally in PtO_2 [30]. The relative atomic concentrations calculated by the integral area referred to Pt(0), Pt(II), and Pt(IV) were 71%, 11%, and 18%, respectively. Obviously, metallic Pt(0) is the predominant species. As for Ru (see Fig. 3d), the Ru 3d peaks overlapped with the C 1s peak, and thus the Ru $3p_{3/2}$ spectrum (at ~463 eV) was chosen for investigation. The Ru $3p_{3/2}$ peak was further separated into three peaks at 462.1, 463.8, and 466.2 eV, corresponding to Ru(0), Ru(IV) in RuO_2, and RuO_xH_y [30],

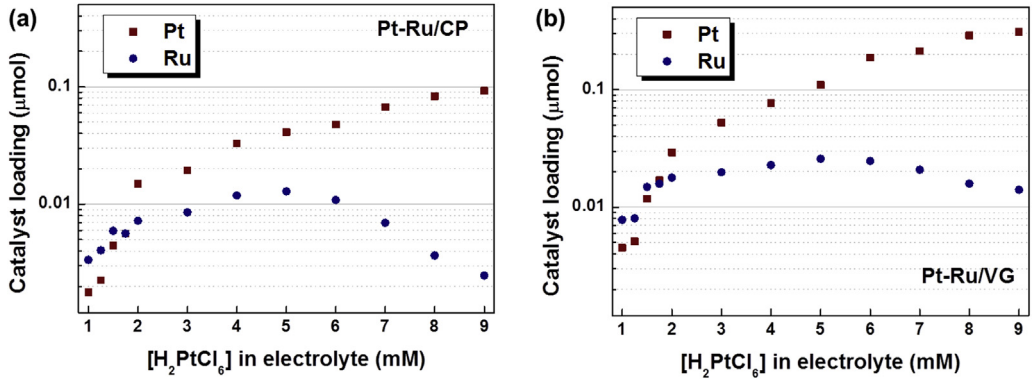

Fig. 1. Pt and Ru loadings on (a) pristine CP and (b) VG-coated CP with a varying electrolyte composition.

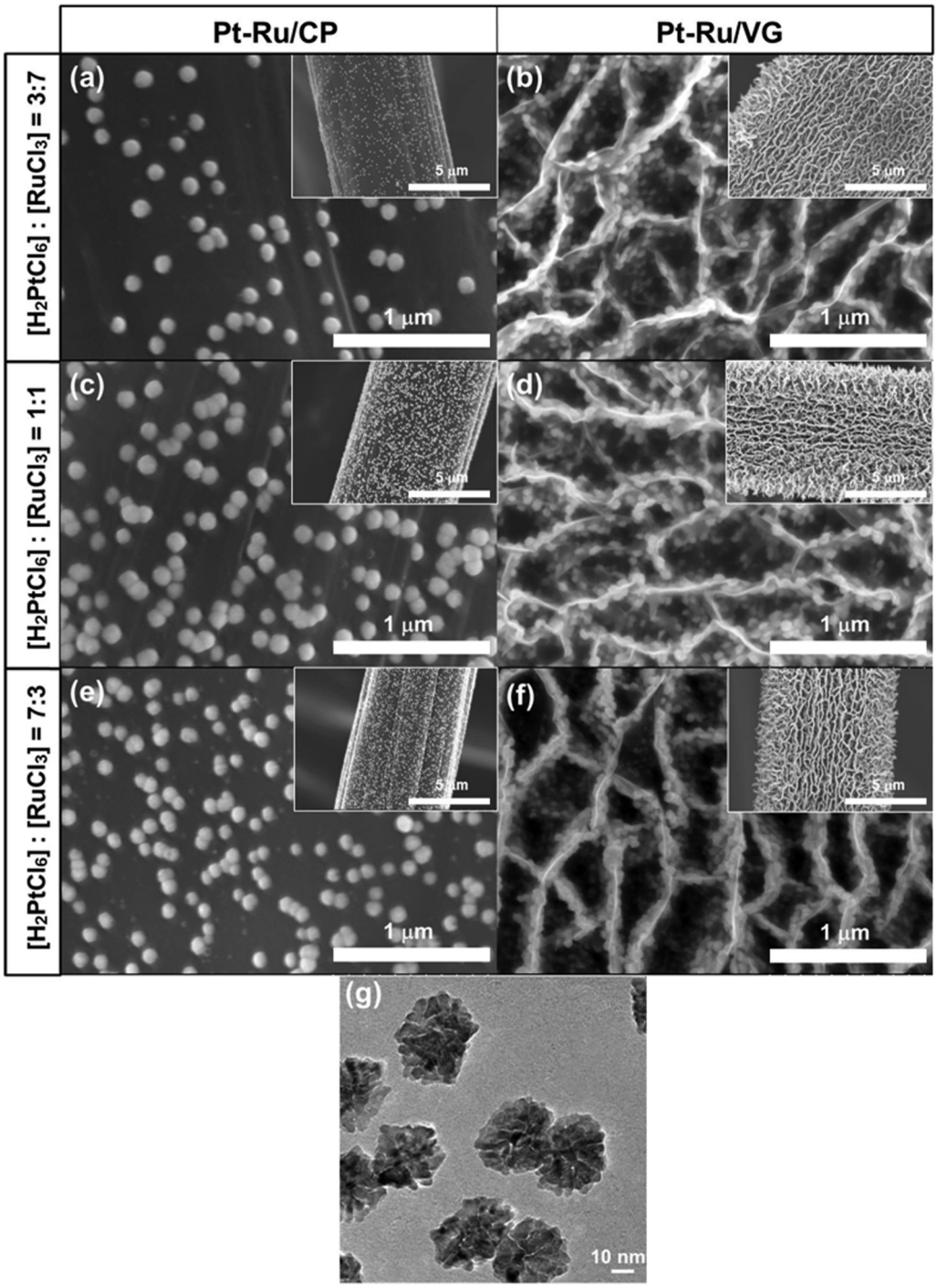

Fig. 2. SEM images of Pt–Ru/CP and Pt–Ru/VG obtained from three typical electrolyte compositions. (a) and (b) $[H_2PtCl_6]$:$[RuCl_3]$ = 3:7, average catalyst diameter: 103.5 ± 3.1 nm and 46.3 ± 1.5 nm; (c) and (d) $[H_2PtCl_6]$:$[RuCl_3]$ = 1:1, average catalyst diameter: 111.1 ± 2.8 nm and 51.2 ± 1.8 nm; (e) and (f) $[H_2PtCl_6]$:$[RuCl_3]$ = 7:3, average catalyst diameter: 98.3 ± 1.9 nm and 45.9 ± 1.1 nm. Insets: SEM images with a smaller magnification. (g) HRTEM image of Pt–Ru/VG obtained from the electrolyte composition of $[H_2PtCl_6]$:$[RuCl_3]$ = 1:1.

respectively. The percentages of Ru(0), RuO_2, and RuO_xH_y were calculated as 76%, 20%, and 4%, respectively, indicating that most of Ru is metallic and alloyed with Pt.

Fig. 4a shows the CV curves of Pt–Ru/VG catalysts in a N_2 saturated solution of 0.5 M H_2SO_4 + 1 M CH_3OH at a scan rate of 50 mV s^{-1}. The as-tested Pt–Ru/VG catalysts were obtained from the electrodeposition with different electrolyte compositions, and thus with different Pt and Ru molar ratios. As is well known, Pt and Ru present very different catalytic abilities toward the dissociative dehydrogenation of methanol, especially at a relatively lower operation temperature [31]. For the current tests operated at room temperature, Pt is considered as the major species responsible for the catalysis of MOR. According to Dickinson et al.'s work, Ru exhibits obvious catalytic ability toward MOR at a temperature of 65 °C [32]. As a consequence, as shown in Fig. 4b, the peak current in the forward scan monotonically increased (indicating an enhanced

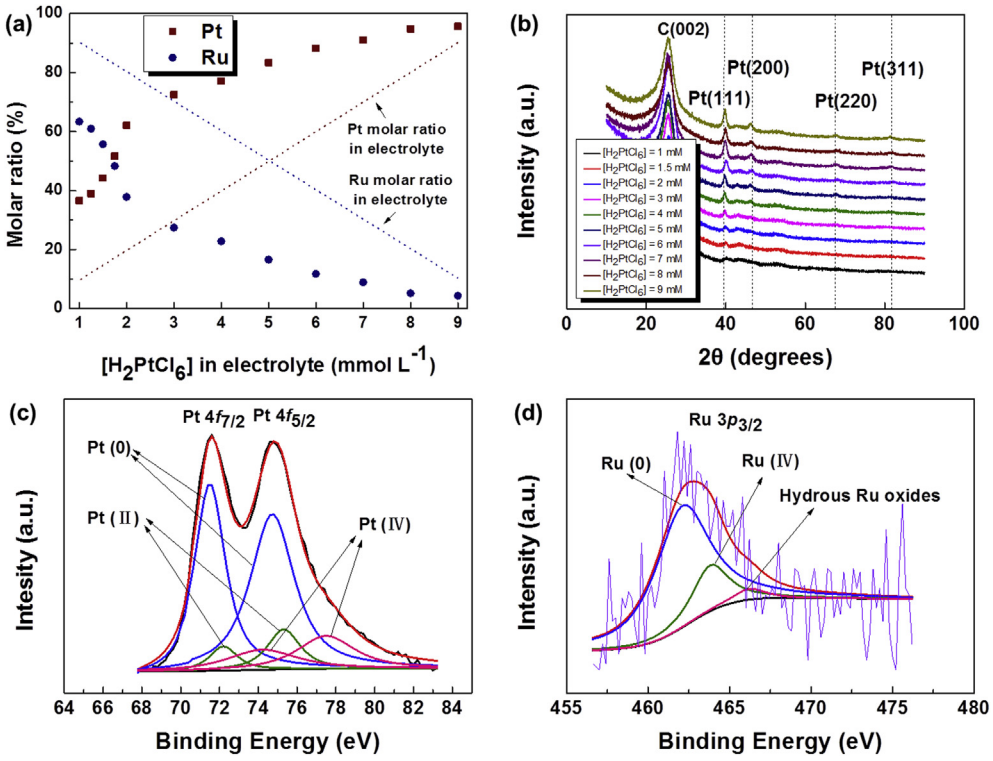

Fig. 3. (a) Molar ratios of Pt and Ru deposited on VG-coated CP with various electrolyte compositions. (b) XRD patterns of Pt–Ru/VG obtained from different electrolyte compositions. (c) Pt 4f XPS spectra and (d) Ru 3p XPS spectra of the catalyst Pt–Ru/VG with a precursor of $[H_2PtCl_6]$:$[RuCl_3]$ = 1:1.

catalytic ability) with the increasing Pt molar ratio. On the other hand, the existence of Ru could enhance the catalytic performance toward MOR through the bifunctional mechanism and electronic effect [9]. It thus explains that, a relatively slow increase of the peak current in the forward scan was observed in the low Ru molar ratio region, as shown in Fig. 4b. For the current work, the highest maximum current density and the smallest corresponding potential were simultaneously achieved at a Pt molar ratio of 83.4%, where the $[H_2PtCl_6]$:$[RuCl_3]$ in the electrolyte was 1:1.

The maximum Pt mass specific catalytic activity at a Pt molar ratio of 83.4% was further corroborated by the electrochemical active surface area (ECSA) calculation. Fig. 5a shows the CV curves of Pt–Ru/VG in a N_2 saturated 0.5 M H_2SO_4 at a scan rate of 50 mV s^{-1}. The Pt ECSA (unit: cm^2 mg^{-1}) was calculated based on the area of hydrogen desorption in the corresponding CV curve:

$$\mathrm{ECSA} = Q_H/(0.21 \times [\mathrm{Pt}]), \quad (1)$$

where Q_H (unit: mC cm^{-2}) is the charge for hydrogen desorption, [Pt] (unit: mg cm^{-2}) is the Pt loading, and 0.21 (unit: mC cm^{-2}) represents the maximum surface charge transferred to Pt during adsorption of monolayer of H. Fig. 5b shows the dependence of Pt ECSA on Pt molar ratio. The highest Pt ECSA was obtained with a Pt molar ratio of 83.4%, consistent with the aforementioned observation shown in Fig. 4b.

3.3. CO resistance and MOR stability of Pt–Ru/VG

Fig. 6a presents the ratio of the maximum current density in the forward scan to that in the backward scan (I_f/I_b) of Pt–Ru/VG obtained from the electrodeposition with different electrolyte compositions. The value of I_f/I_b can be used as an index to evaluate the catalyst tolerance to the poisoning species [33,34]. The Pt–Ru/VG catalyst with a Pt molar ratio of 83.4% presented the highest I_f/I_b value of 3.30 among all the catalysts, indicating the most effective removal of poisoning species on the catalyst surface. Previous work

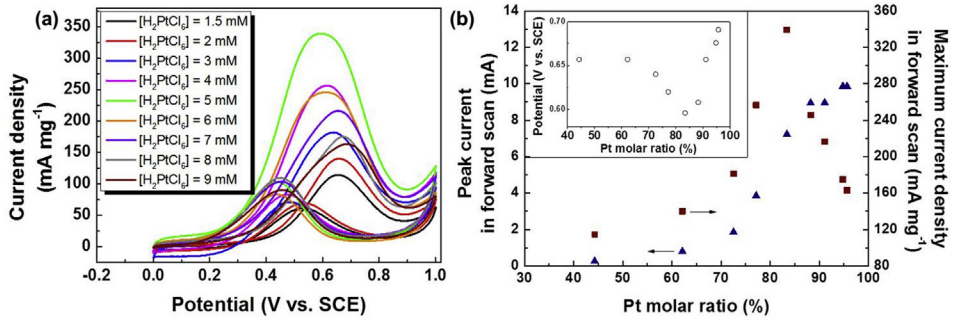

Fig. 4. (a) CV curves of Pt–Ru/VG in a N_2 saturated solution of 0.5 M H_2SO_4 + 1 M CH_3OH at a scan rate of 50 mV s^{-1}. (b) Dependences of the peak current and maximum current density in the forward scan on the Pt molar ratio. Inset: potential of MOR peak current for Pt–Ru/VG with different Pt molar ratios.

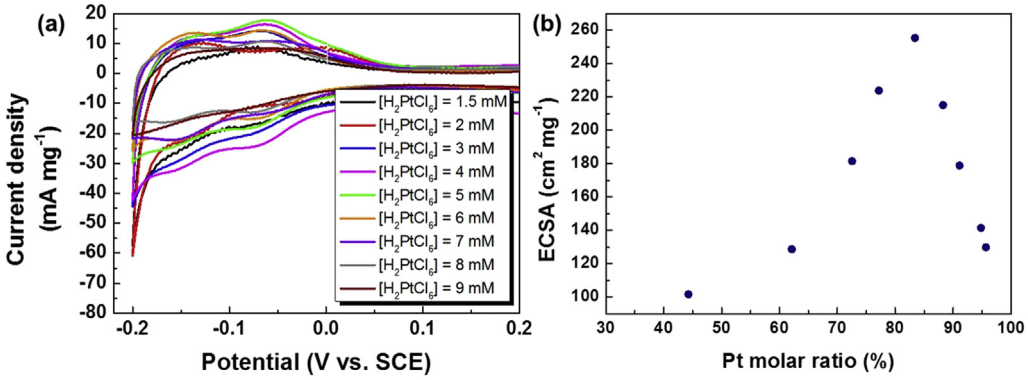

Fig. 5. (a) CV curves of Pt–Ru/VG in a N_2 saturated solution of 0.5 M H_2SO_4 at a scan rate of 50 mV s^{-1}. (b) Dependence of Pt ECSA on Pt molar ratio.

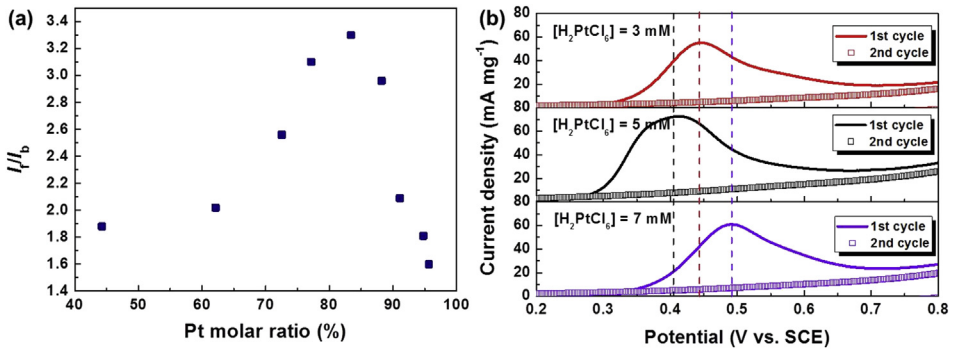

Fig. 6. (a) I_f/I_b of Pt–Ru/VG catalysts with different Pt molar ratios. (b) CO stripping voltammograms in 0.5 M H_2SO_4 solution at a scan rate of 50 mV s^{-1} recorded for the Pt–Ru/VG catalysts obtained from three typical electrolyte compositions.

reveals that $Pt_3{\equiv}C{-}OH$ and CO_{ads} are the major metastable and stable intermediates [3], and the presence of Ru can lead to the formation of active OH_{ads} at a low potential to react with the adsorbed intermediates on neighboring Pt sites, as shown by the following reactions [35,36]:

$$Ru + H_2O \rightarrow Ru{-}(OH)_{ads} + H^+ + e^- \quad (R1)$$

$$Ru{-}(OH)_{ads} \rightarrow Ru{-}O + H^+ + e^- \quad (R2)$$

$$Ru{-}O + Pt_3{\equiv}C{-}OH \rightarrow Ru + 3Pt + CO_2 + H^+ + e^- \quad (R3)$$

$$Ru{-}(OH)_{ads} + Pt{-}(CO)_{ads} \rightarrow Ru + Pt + CO_2 + 2H^+ + e^- \quad (R4)$$

However, the I_f/I_b values of Ru rich catalysts (e.g., Pt molar ratio of 44.3%) were relatively low, consistent with the previously reported observation [37] and probably due to the poor catalytic activity of Ru at room temperature.

Efficient removal of the poisoning species such as CO from the catalyst is of great significant for evaluating the catalyst performance in DMFCs. Oxidation of CO_{ads} was thus measured by CO stripping voltammetry in 0.5 M H_2SO_4 solution at a scan rate of 50 mV s^{-1}. To allow the complete adsorption of CO onto catalysts, CO was purged into the cell for 30 min with maintaining a constant voltage of 100 mV vs. SCE. Then N_2 was used to purge out the excess CO dissolved in the electrolyte for 30 min. Fig. 6b shows the voltammograms of CO_{ads} oxidation on the Pt–Ru/VG catalysts obtained from three typical electrolyte compositions, *i.e.*, $[H_2PtCl_6]$:$[RuCl_3]$ = 3:7, $[H_2PtCl_6]$:$[RuCl_3]$ = 1:1, and $[H_2PtCl_6]$:$[RuCl_3]$ = 7:3, respectively. The distinct CO oxidation peak appeared during the first forward scan whereas disappears in the second forward scan, manifesting that the adsorbed CO on the surface of Pt–Ru nanoparticles has been oxidized during the first forward scan [38,39]. The Pt–Ru/VG with an initial $[H_2PtCl_6]$ of 5 mM exhibited the lowest peak potential (~0.41 V vs. SCE), indicating the best CO tolerance.

Stability measurements of three typical Pt–Ru/VG catalysts were performed by CA measurements in 0.5 M H_2SO_4 + 1.0 M CH_3OH solution on catalysts at 0.6 V vs. SCE for 900 s. As shown in Fig. 7, the current presented an ultrafast decay at the initial period and then reached a pseudo steady state. The high initial current was

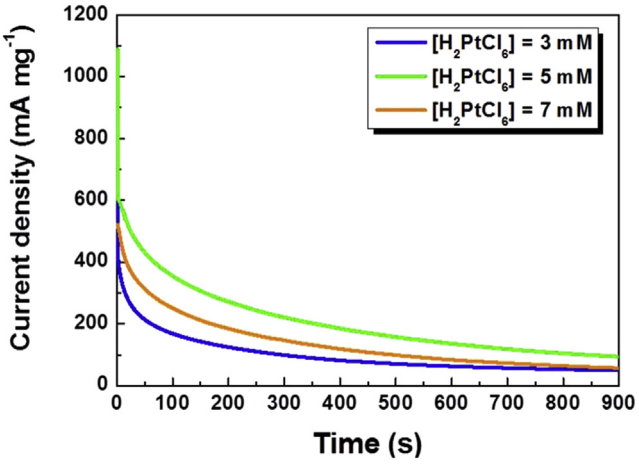

Fig. 7. Chronoamperometry measurements of Pt–Ru/VG catalysts in 0.5 M H_2SO_4 + 1.0 M CH_3OH solution at 0.6 V vs. SCE for 900 s.

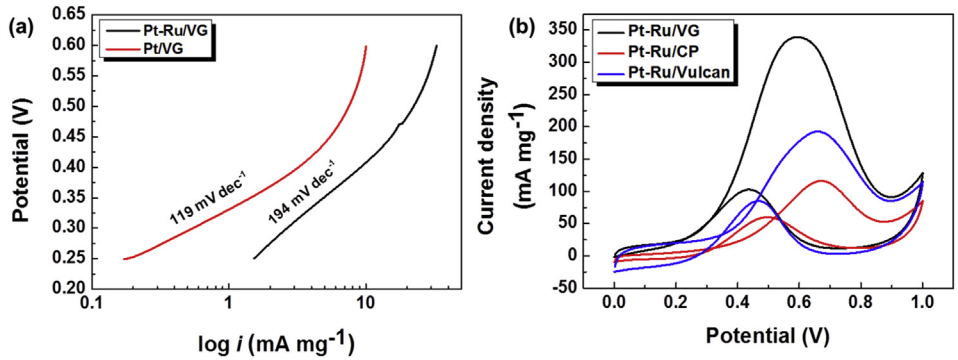

Fig. 8. (a) Tafel curves of Pt/VG and Pt–Ru/VG. (b) CV curves of Pt–Ru/VG, Pt–Ru/CP, and Pt–Ru/Vulcan in a N_2 saturated solution of 0.5 M H_2SO_4 + 1 M CH_3OH at a scan rate of 50 mV s^{-1}.

due to double layer charge and the sufficient active sites on those catalysts for MOR. The following quick decay of current is mainly attributed to the blocking of active sites by the poisoning species and intermediate products. The Pt–Ru/VG catalyst obtained with an initial [H_2PtCl_6] of 5 mM exhibited the highest initial/steady current and the lowest current decay rate, demonstrating the best catalytic stability and poisoning tolerance.

3.4. Comparison with Pt/VG, Pt–Ru/CP, and Pt–Ru/Vulcan

Tafel curves (potential vs. log *i*) were plotted to compare the MOR kinetics of Pt/VG and Pt–Ru/VG. An electrolyte with 10 mM H_2PtCl_6 + 0.5 M H_2SO_4 was applied for the electrodeposition of Pt on VG. The Pt–Ru/VG catalyst was obtained with an initial [H_2PtCl_6] of 5 mM. The charge transfer coefficient (α) was calculated from the slope of each curve. As shown in Fig. 8a, the Tafel plots can be divided into two nearly linear regions that intersect at approximately 0.45 V for both catalysts, indicating a change in the rate-determining steps. In the region below 0.45 V, the Tafel slope of Pt/VG was 119 mV dec^{-1} (α = 0.50), very close to the theoretical value predicted for one-electron transfer reaction as rate determining step [40]. However, for Pt–Ru/VG, the Tafel slope in the same region was much higher, *i.e.*, 194 mV dec^{-1} (α = 0.31), indicating a faster methanol dehydrogenation even at the relatively low overpotential region [41]. The exchange current density of Pt–Ru/VG (4.11 μA cm^{-2}), calculated based on the Tafel curves [40], was found to be nearly one order of magnitude higher than that of Pt/VG (0.64 μA cm^{-2}).

The electrochemical performance of Pt–Ru/VG was further compared with those of Pt–Ru/CP and Pt–Ru/Vulcan. The electrodeposition of Pt–Ru catalysts on all the supports was conducted using the same electrolyte composition of [H_2PtCl_6]:[$RuCl_3$] = 1:1. Fig. 8b shows the CV curves of Pt–Ru/VG, Pt–Ru/CP, and Pt–Ru/Vulcan in a N_2 saturated solution of 0.5 M H_2SO_4 + 1 M CH_3OH at a scan rate of 50 mV s^{-1}. It was observed that, the Pt–Ru/VG catalyst possessed of a maximum current density of 339.2 mA mg^{-1}, significantly higher than those of Pt–Ru/CP and Pt–Ru/Vulcan (116.3 and 192.8 mA mg^{-1}, respectively) and thus presenting a much enhanced catalytic activity toward MOR. Compared with the previously reported data, this value is higher than that of Pt–Ru/CP prepared with the one-step coelectrodeposition method (~40 mA mg^{-1}) where the size of Pt–Ru nanoparticles is at the same level as the current work (few tens of nanometers) [42]. Meanwhile, the maximum current density of Pt–Ru/VG is also higher than some of Pt–Ru/Vulcan and Pt–Ru/CNTs produced with microwave-polyol and ethylene glycol reduction methods [38,43]. As is well known, the repeated pulse potentials approach owns the advantageous in achieving nanoparticles with a good control and selectivity in the nanoparticle size and dispersion [44], while the size of nanoparticles is usually much larger than those produced by magnetron dc sputtering and solution-reduction [17,20]. Based on the total mass of Pt and Ru, the maximum current density of Pt–Ru/VG in the current work was calculated as 302.3 mA mg^{-1}, higher than those reported in Refs. [38] and [43] (both of which are less than 200 mA mg^{-1}), although with a much larger size of nanoparticles. However, the currently presented activities of Pt–Ru/VG are still poorer than some practices employing catalysts with much smaller size [45,46]. Further improvement on the catalytic performance of Pt–Ru/VG appears likely through the preparation of smaller catalyst nanoparticles *via* chemical routes. Previous work has proved that Pt nanoparticles with a mean size of few nanometers can be decorated on VG surface *via* a solution-reduction method [47]. Furthermore, the Pt–Ru/VG presented the smallest potential for peak current density (0.596, 0.676 and 0.659 V for Pt–Ru/VG, Pt–Ru/CP, and Pt–Ru/Vulcan, respectively) and the highest I_f/I_b value (3.30, 1.94 and 2.22 for Pt–Ru/VG, Pt–Ru/CP, and Pt–Ru/Vulcan, respectively).

4. Conclusions

Taking the advantages of non-stacking morphology and exposed graphene edge planes, VG-coated CP could work as a better support than pristine CP, exhibiting higher catalyst loading, smaller catalyst size, and improved nanoparticle dispersion. With adjusting the electrolyte composition (*i.e.*, H_2PtCl_6 and $RuCl_3$ concentrations), the molar ratios of Pt and Ru in the deposits were well controlled. For Pt–Ru/VG, the bulk catalytic ability increased with an increasing Pt molar ratio in the deposits, while the best mass specific activity, CO tolerance, and catalytic stability were synthetically achieved at a Pt molar ratio of 83.4% in the deposits ([H_2PtCl_6]:[$RuCl_3$] = 1:1 in the electrolyte). The Tafel analysis indicated that Pt–Ru/VG realized a faster methanol dehydrogenation than Pt/VG. Meanwhile, Pt–Ru/VG presented a maximum current density of 339.2 mA mg^{-1}, not only significantly higher than the Pt–Ru/CP and Pt–Ru/Vulcan counterparts obtained with the same repeated pulse potentials method, but also higher than some of the previously reported Pt–Ru/Vulcan and Pt–Ru/CNTs catalysts with smaller nanoparticle size. The above observation implies that Pt–Ru/VG with an optimized Pt and Ru molar ratio could be a very promising anode catalyst for high-performance MOR. Future improvement on the morphology and structure of VG support as well as more comprehensive measurements (such as single cell test) on the catalytic performance will be considered in our future work.

Acknowledgements

The authors acknowledge the financial support from the National Natural Science Foundation of China (No. 51306159), the Zhejiang Provincial Natural Science Foundation of China (No. LY13E020004), the Foundation of National Excellent Doctoral Dissertation of China (No. 201238), the Specialized Research Fund for the Doctoral Program of Higher Education (No. 20120101120140), and the Fundamental Research Funds for the Central Universities (No. 2014FZA4011).

References

[1] S. Wasmus, A. Kuver, J. Electroanal. Chem. 461 (1999) 14–31.
[2] H.S. Liu, C.J. Song, L. Zhang, J.J. Zhang, H.J. Wang, D.P. Wilkinson, J. Power Sources 155 (2006) 95–110.
[3] P.S. Kauranen, E. Skou, J. Munk, J. Electroanal. Chem. 404 (1996) 1–13.
[4] V.S. Bagotzky, Y.B. Vassilyev, Electrochim. Acta 12 (1967) 1323–1343.
[5] V. Selvaraj, M. Alagar, Electrochem. Commun. 9 (2007) 1145–1153.
[6] L. Dai, D.W. Chang, J.-B. Baek, W. Lu, Small 8 (2012) 1130–1166.
[7] M. Watanabe, S. Motto, J. Electroanal. Chem. 60 (1975) 267–273.
[8] T. Frelink, W. Visscher, J.A.R. Vanveen, Surf. Sci. 335 (1995) 353–360.
[9] X. Zhao, M. Yin, L. Ma, L. Liang, C. Liu, J. Liao, T. Lu, W. Xing, Energ. Envrion. Sci. 4 (2011) 2736–2753.
[10] A.S. Arico, S. Srinivasan, V. Antonucci, Fuel Cells 1 (2001) 133–161.
[11] B.R. Cuenya, Thin Solid Films 518 (2010) 3127–3150.
[12] M. Liu, R. Zhang, W. Chen, Chem. Rev. 114 (2014) 5117–5160.
[13] S. Sharma, B.G. Pollet, J. Power Sources 208 (2012) 96–119.
[14] H. Tang, J.H. Chen, Z.P. Huang, D.Z. Wang, Z.F. Ren, L.H. Nie, Y.F. Kuang, S.Z. Yao, Carbon 42 (2004) 191–197.
[15] R. Wu, Y. Xue, X. Qian, H. Liu, K. Zhou, S.H. Chan, J.N. Tey, J. Wei, B. Zhu, Y. Huang, Int. J. Hydrogen Energy 38 (2013) 16677–16684.
[16] Z. Bo, Y. Yang, J. Chen, K. Yu, J. Yan, K. Cen, Nanoscale 5 (2013) 5180–5204.
[17] C. Zhang, J. Hu, X. Wang, X. Zhang, H. Toyoda, M. Nagatsu, Y. Meng, Carbon 50 (2012) 3731–3738.
[18] X. Zhang, E. Wu, D. Hu, Z. Bo, W. Zhu, K. Yu, C. Yu, Z. Wang, J. Yan, K. Cen, Phys. Status Solidi B 251 (2014) 829–837.
[19] L. Giorgi, T.D. Makris, R. Giorgi, N. Lisi, E. Salernitano, Sens. Actuators, B 126 (2007) 144–152.
[20] N. Soin, S.S. Roy, T.H. Lim, J.A.D. McLaughlin, Mater. Chem. Phys. 129 (2011) 1051–1057.
[21] Z. Bo, W. Zhu, W. Ma, Z. Wen, X. Shuai, J. Chen, J. Yan, Z. Wang, K. Cen, X. Feng, Adv. Mater. 25 (2013) 5799–5806.
[22] Y. Ra, J. Lee, I. Kim, S. Bong, H. Kima, J. Power Sources 187 (2009) 363–370.
[23] C. Yang, D. Wang, X. Hu, C. Dai, L. Zhang, J. Alloys Compd. 448 (2008) 109–115.
[24] L. Gan, H. Du, B. Li, F. Kang, J. Power Sources 191 (2009) 233–239.
[25] E.A. Franceschini, M.M. Bruno, F.J. Williams, F.A. Viva, H.R. Corti, ACS Appl. Mater. Interfaces 5 (2013) 10437–10444.
[26] J.-J. Jow, S.-W. Yang, H.-R. Chen, M.-S. Wu, T.-R. Ling, T.-Y. Wei, Int. J. Hydrogen Energ. 34 (2009) 665–671.
[27] S. Sen, F. Sen, G. Gokagac, Phys. Chem. Chem. Phys. 13 (2011) 6784–6792.
[28] S. Rojas, F.J. Garcia-Garcia, S. Jaras, M.V. Martinez-Huerta, J.L.G. Fierro, M. Boutonnet, Appl. Catal., A: Gen. 285 (2005) 24–35.
[29] E. Antolini, F. Cardellini, L. Giorgi, E. Passalacqua, J. Mater. Sci. Lett. 19 (2000) 2099–2103.
[30] J.-N. Zheng, S.-S. Li, F.-Y. Chen, N. Bao, A.-J. Wang, J.-R. Chen, J.-J. Feng, J. Power Sources 266 (2014) 259–267.
[31] H.A. Gasteiger, N. Markovic, P.N. Ross, E.J. Cairns, J. Electrochem. Soc. 141 (1994) 1795–1803.
[32] A.J. Dickinson, L.P.L. Carrette, J.A. Collins, K.A. Friedrich, U. Stimming, J. Appl. Electrochem. 34 (2004) 975–980.
[33] Y.Y. Mu, H.P. Liang, J.S. Hu, L. Jiang, L.J. Wan, J. Phys. Chem. B 109 (2005) 22212–22216.
[34] L. Feng, G. Gao, P. Huang, X. Wang, C. Zhang, J. Zhang, S. Guo, D. Cui, Nanoscale Res. Lett. 6 (2011).
[35] R.K. Raman, A.K. Shukla, A. Gayen, M.S. Hegde, K.R. Priolkar, P.R. Sarode, S. Emura, J. Power Sources 157 (2006) 45–55.
[36] P. Gajendran, R. Saraswathi, J. Solid State Electrochem. 17 (2013) 2741–2747.
[37] Z.L. Liu, X.Y. Ling, X.D. Su, J.Y. Lee, J. Phys. Chem. B 108 (2004) 8234–8240.
[38] S. Jiang, L. Zhu, Y. Ma, X. Wang, J. Liu, J. Zhu, Y. Fan, Z. Zou, Z. Hu, J. Power Sources 195 (2010) 7578–7582.
[39] M.-S. Kim, B. Fang, N.K. Chaudhari, M. Song, T.-S. Bae, J.-S. Yu, Electrochim. Acta 55 (2010) 4543–4550.
[40] A. Velazquez-Palenzuela, F. Centellas, J. Antonio Garrido, C. Arias, R. Maria Rodriguez, E. Brillas, P.-L. Cabot, J. Power Sources 196 (2011) 3503–3512.
[41] X. Lu, J. Hu, J.S. Foord, Q. Wang, J. Electroanal. Chem. 654 (2011) 38–43.
[42] S.H. Ahn, I. Choi, O.J. Kwon, J.J. Kim, Chem. Eng. J. 181 (2012) 276–280.
[43] L. Gan, R. Lv, H. Du, B. Li, F. Kang, Electrochem. Commun. 11 (2009) 355–358.
[44] T. Maiyalagan, X. Dong, P. Chen, X. Wang, J. Mater. Chem. 22 (2012) 5286–5290.
[45] C. Ma, W. Liu, M. Shi, X. Lang, Y. Chu, Z. Chen, D. Zhao, W. Lin, C. Hardacre, Electrochim. Acta 114 (2013) 133–141.
[46] S. Zhao, H. Yin, L. Du, G. Yin, Z. Tang, S. Liu, J. Mater. Chem. A 2 (2014) 3719–3724.
[47] S. Chul Shin, A. Yoshimura, T. Matsuo, M. Mori, M. Tanimura, A. Ishihara, K.-i. Ota, M. Tachibana, J. Appl. Phys. 110 (2011) 104308.